

A stepwise model for double-stranded RNA processing by ribonuclease III

Jianhua Gan, Gary Shaw, Joseph E. Tropea,
David S. Waugh, Donald L. Court and Xinhua Ji*
Center for Cancer Research, National Cancer Institute,
National Institutes of Health, Frederick, MD 21702, USA.

Summary

RNA interference is mediated by small interfering RNAs produced by members of the ribonuclease III (RNase III) family represented by bacterial RNase III and eukaryotic Rnt1p, Drosha and Dicer. For mechanistic studies, bacterial RNase III has been a valuable model system for the family. Previously, we have shown that RNase III uses two catalytic sites to create the 2-nucleotide (nt) 3' overhangs in its products. Here, we present three crystal structures of RNase III in complex with double-stranded RNA, demonstrating how Mg²⁺ is essential for the formation of a catalytically competent protein–RNA complex, how the use of two Mg²⁺ ions can drive the hydrolysis of each phosphodiester bond, and how conformational changes in both the substrate and the protein are critical elements for assembling the catalytic complex. Moreover, we have modelled a protein–substrate complex and a protein–reaction intermediate (transition state) complex on the basis of the crystal structures. Together, the crystal structures and the models suggest a stepwise mechanism for RNase III to execute the phosphoryl transfer reaction.

Introduction

The ribonuclease III (RNase III) family is represented by bacterial RNase III and eukaryotic Rnt1p, Drosha and Dicer (Blaszczuk *et al.*, 2001; Conrad and Rauhut, 2002; Nicholson, 2003; Ji, 2006), among which the bacterial RNase III, discovered in 1968 (Robertson *et al.*, 1968), is the most studied family member (Court, 1993; Nicholson, 1999; Conrad and Rauhut, 2002; 2003; Ji, 2006; 2007). RNase III proteins are Mg²⁺-dependent, double-stranded RNA (dsRNA)-specific endonucleases, characterized by a nine-residue signature motif in their endonuclease

domain (endoND) and a 2-nucleotide (nt) 3' overhang in their product (Robertson *et al.*, 1968; Court, 1993; Nicholson, 1996; Krainer, 1997; 1999; Filippov *et al.*, 2000). They play important roles in RNA processing (Robertson *et al.*, 1968), post-transcriptional gene expression control (Court, 1993; Krainer, 1997; Wu *et al.*, 2000) and defence against viral infection (Saleh *et al.*, 2004; van Rij and Andino, 2006).

Dicer is a dsRNA-processing enzyme, producing small interfering RNAs (siRNAs) that mediate RNA interference (RNAi) (Bernstein *et al.*, 2001; Carthew, 2001). Bacterial RNase III can function as either a dsRNA-processing enzyme or a dsRNA-binding protein. As a processing enzyme, it cleaves both natural and synthetic dsRNA into small duplexes; as a binding protein, it binds and stabilizes certain RNAs without cleaving them (Guarneros, 1988; Court, 1993; Oppenheim *et al.*, 1993; Dasgupta *et al.*, 1998; Calin-Jageman and Nicholson, 2003). *In vitro*, both Dicer and bacterial RNase III can be used to produce siRNA cocktails as effective RNAi mediators (Yang *et al.*, 2002). Structurally, however, Dicer [~2000 amino acid (aa) residues] is much more complicated than bacterial RNase III (~200 aa residues). A typical Dicer protein contains an RNA helicase domain, a PAZ (Piwi Argonaute Zwiile) domain, two endoNDs and one dsRNA-binding domain (dsRBD) (Bernstein *et al.*, 2001), whereas bacterial RNase III is composed of a single endoND followed by a dsRBD (Robertson *et al.*, 1968). Therefore, bacterial RNase III provides the best-known model for evaluating the mechanistic details of RNase III activity (Gan *et al.*, 2006; Ji, 2007).

Previously, we have shown that the structures of non-catalytic and catalytic complexes of bacterial RNase III with dsRNA are dramatically different (Blaszczuk *et al.*, 2004; Gan *et al.*, 2006). We have also shown how RNase III uses two catalytic sites to create a 2 nt 3' overhang in the product (Gan *et al.*, 2006). Briefly, the dimerization of the endoND is essential for the function of RNase III enzymes because it creates a catalytic valley where the catalytic sites are located. The catalytic valley accommodates a dsRNA in a manner such that each of the two RNA strands is aligned with one of the two catalytic sites. The hydrolysis of each strand involves both subunits; residues from one subunit are involved in the selection of the scissile bond, while those from the partner subunit are involved in the cleavage chemistry.

Accepted 27 October, 2007. *For correspondence. E-mail jix@ncifcrf.gov; Tel. (+1) 301 846 5035; Fax (+1) 301 846 6073.

Table 1. Sequence of the substrate and product RNAs of Aa-RNase III.

RNA	Sequence	No. nt
5 ^a	5'-AUAAGGUCAUUC-GCAA-GAGUGGCCUUUAU-3'	30
6 ^a	5'-AAAGGUCAUUC-GCAA-GAGUGGCCUUUAU-3'	28
7 ^b	5'-GGGACAAGCGCAAGGUCAUUC-GCAA-GAGUGGCCUUGCGCUUGUCCC-3'	46
8	5'-CAAGGUCAUUC-GCAA-GAGUGGCCUUGCG-3'	28
9	5'-AAGGUCAUUC-G & AGUGGCCUUGC-3'	2 × 11

a. Gan *et al.* (2006).

b. Derived in part from R1.1[WC] var-7 RNA (Zhang and Nicholson, 1997).

RNase III enzymes belong to a superfamily of polynucleotidyl transferases that include RNases, DNases and transposases. A two-metal-ion catalytic mechanism has been established for Tn5 transposase (Davies *et al.*, 2000; Steiniger-White *et al.*, 2004) and ribonuclease H (RNase H) (Nowotny *et al.*, 2005; Nowotny and Yang, 2006), and predicted for RNase III (Sun *et al.*, 2005; Ji, 2006; MacRae *et al.*, 2006a). Previously, however, only one Mg²⁺ has been observed in each of the two catalytic sites in a catalytically compatible protein–RNA complex of the D44N mutant of *Aquifex aeolicus* RNase III (Aa-RNase III) (PDB entry 2EZ6, Gan *et al.*, 2006). Comparison between the catalytic site of Aa-RNase III(D44N) with that of RNase H indicates that the D44 residue of wild-type Aa-RNase III would be positioned to bind a second Mg²⁺ ion (Gan *et al.*, 2006). Recently, a Mn²⁺ or an Er³⁺ ion has been found in this position in an RNA-free Dicer structure (MacRae *et al.*, 2006a). An intriguing question is therefore whether the D44N mutation hindered the binding of a second Mg²⁺ ion in the protein–RNA complex. This question prompted us to carry out experiments with wild-type Aa-RNase III, and at the same time, to test the role of Mg²⁺ in the formation of catalytically competent protein–RNA complexes. Here, we present three new structures, including a snapshot of the catalytic complex immediately after the phosphoryl transfer during the hydrolysis of a phosphodiester bond.

Results and discussion

In the following sections, we will use the aa residue numbers for Aa-RNase III unless otherwise stated. The RNA sequences are summarized in Table 1.

Mg²⁺ is essential for the catalytic binding of RNA

Catalytic anti-determinants (negative determinants), which uncouple the RNA binding and processing activities of RNase III, can be either a special structural motif embedded in the RNA (Dasgupta *et al.*, 1998; Calin-Jageman *et al.*, 2001; Calin-Jageman and Nicholson, 2003) or a defect caused by mutation in the protein (Inada and Nakamura, 1995; Blaszczyk *et al.*, 2004). In both cases, it is the interaction between the catalytic valley and

the RNA that is disrupted. We have shown previously, unlike most other RNA/DNA-binding proteins, the catalytic valley of RNase III is highly negatively charged, and thus the bound Mg²⁺ is critical in the formation and stabilization of the catalytic site assembly (Blaszczyk *et al.*, 2001; 2004). We have also shown that, for dsRNA processing, the substrate must be bound in the catalytic valley (Gan *et al.*, 2006). We show here that, for this binding specificity, Mg²⁺ is a positive determinant.

When Mg²⁺ is absent (see crystallization conditions, Table 2), RNA 7, a 46-mer stem-loop RNA, is bound by the protein outside of the catalytic valley (Fig. 1A). The overall conformation of the Aa-RNase II–RNA 7 complex is identical to that of a non-catalytic complex of the Aa-RNase III(E110K) mutant with a self-complementary RNA duplex of the sequence 5'-GGCGCGCGCC-3' (RNA 1) which we reported previously (PDB entry 1RC7, Blaszczyk *et al.*, 2004). Both the protein (the wild type versus the E110K mutant) and the RNA (RNA 7 versus RNA 1) are different in the two protein–RNA complexes [Aa-RNase III–RNA 7 and Aa-RNase III(E110K)–RNA 1], and either the absence of Mg²⁺ or the E110K mutation, respectively, inhibits the binding of dsRNA in the catalytic valley. These results are consistent with the effect of the E110K mutation as a negative determinant, and the Mg²⁺ ion as a positive determinant for substrate binding to the catalytic valley.

When Mg²⁺ is present (Table 2), RNA 7 is bound in the catalytic valley and cleaved to generate RNA 8 as observed in the crystal structure of Aa-RNase III–MgRNA 8 (Fig. 1B), which is similar to the Aa-RNase III(D44N)–MgRNA 6 structure (PDB entry 2EZ6) obtained by incubating the protein with RNA 5 (Table 1), another substrate of the enzyme (Gan *et al.*, 2006). However, only one Mg²⁺ ion per catalytic site has been found in the Aa-RNase III(D44N)–MgRNA 6 structure, whereas two per catalytic site have been identified in the Aa-RNase III–MgRNA 8 structure.

The two Mg²⁺ ions are located in close proximity to each scissile bond in the Aa-RNase III–MgRNA 8 structure (Fig. 1C). One of them (designated as MgA) co-ordinates with three aa side-chains (E110, E40 and D107) and two water molecules while the other (designated as MgB) co-ordinates with two side-chains (E110 and D44) and one

Table 2. Crystallization, X-ray diffraction data, structure solution and refinement statistics.

Protein	Aa-RNase III	Aa-RNase III	Aa-RNase III
RNA			
Substrate	RNA 7 ^a	RNA 7	RNA 8
Product		RNA 8	RNA 9
Protein–RNA complex	Aa-RNase III–RNA 7 (Fig. 1A)	Aa-RNase III–MgRNA 8 (Fig. 1B)	Aa-RNase III–MgRNA 9 (Fig. 2B)
Crystallization			
Protein solution (PS)	0.4 mM Aa-RNase III 0.4 mM RNA 7 300 mM NaCl and 25 mM Tris, pH 7.2	0.4 mM Aa-RNase III 0.8 mM RNA 7 400 mM NaCl 50 mM MgCl ₂ 25 mM Tris, pH 7.2	0.4 mM Aa-RNase III 0.8 mM RNA 8 100 mM NaCl 50 mM MgCl ₂ 25 mM Tris, pH 7.2
Reservoir solution (RS)	0.2 M NaCl 16–17% PEG3350 0.1 M Tris, pH 8.5	0.2 M NaCl 25% w/v PEG 3350 0.1 M Tris, pH 8.5	3.4 M 1,6-hexanediol 0.2 M MgCl ₂ 0.1 M Tris, pH 8.5
Drop size (μl)	2 PS + 1 RS	0.2 PS + 0.2 RS	2 PS + 2 RS
X-ray diffraction data			
Space group	C2	P2 ₁	P2 ₁ 2 ₁ 2
Unicell parameter: a (Å)	101.6	64.1	96.4
Unicell parameter: b (Å)	101.7	51.1	119.9
Unicell parameter: c (Å)	67.1	113.4	58.9
Unicell parameter: α (°)	90.0	90.0	90.0
Unicell parameter: β (°)	103.7	104.9	90.0
Unicell parameter: γ (°)	90.0	90.0	90.0
Resolution (Å)	2.9–30.0 (2.9–3.0)	2.5–30.0 (2.5–2.66)	1.7–30.0 (1.7–1.76)
Completeness (%) (last shell)	89.1 (53.4)	84.5 (62.6)	89.6 (62.2)
I/σ(I) (last shell)	13.3 (3.4)	8.5 (2.9)	22.2 (2.8)
R _{merge} (%) (last shell) ^b	7.2 (16.0)	9.3 (23.7)	5.1 (23.1)
Structure solution			
Method or program	AMoRe ^c	AMoRe	PHASER ^d
Search or starting model	PDB entry 1RC7	PDB entry 2EZ6	PDB entry 1RC7
Refinement statistics			
No. of data for refinement	12473	19932	67277
No. of data for R _{free}	669	1030	3425
No. of amino acid residues/atoms	440/3675	438/3660	434/3627
No. of nt residues/atoms	46/980	56/1200	44/1034
No. of Mg ²⁺ ions	0	8	19
No. of solvent (water) oxygens	36	122	445
R-factor (%) ^e	23.7	22.2	19.4
R _{free} (%) ^f	27.6	28.4	21.9
Overall B factor (Å ²)	98.0	56.8	33.0
Wilson B factor (Å ²)	72.4	49.6	23.2
RMSD			
Bond distances (Å)	0.004	0.007	0.005
Bond angles (°)	0.8	1.2	1.0
Ramachandran statistics (%)			
Most favoured φ/ψ values	81.8	92.6	94.5
Additional allowed φ/ψ values	16.9	6.4	5.0
Disallowed φ/ψ values	0	0	0

a. See Table 1 for RNA sequence.

b. $R_{\text{merge}} = \sum(I - \langle I \rangle) / \sum I$, where I is the observed intensity.

c. Molecular replacement program (Navaza, 1994).

d. Molecular replacement program (Reed, 2000).

e. R-factor = $\sum_{hkl} | |F_o| - |F_c| | / \sum_{hkl} |F_o|$, calculated from working dataset.

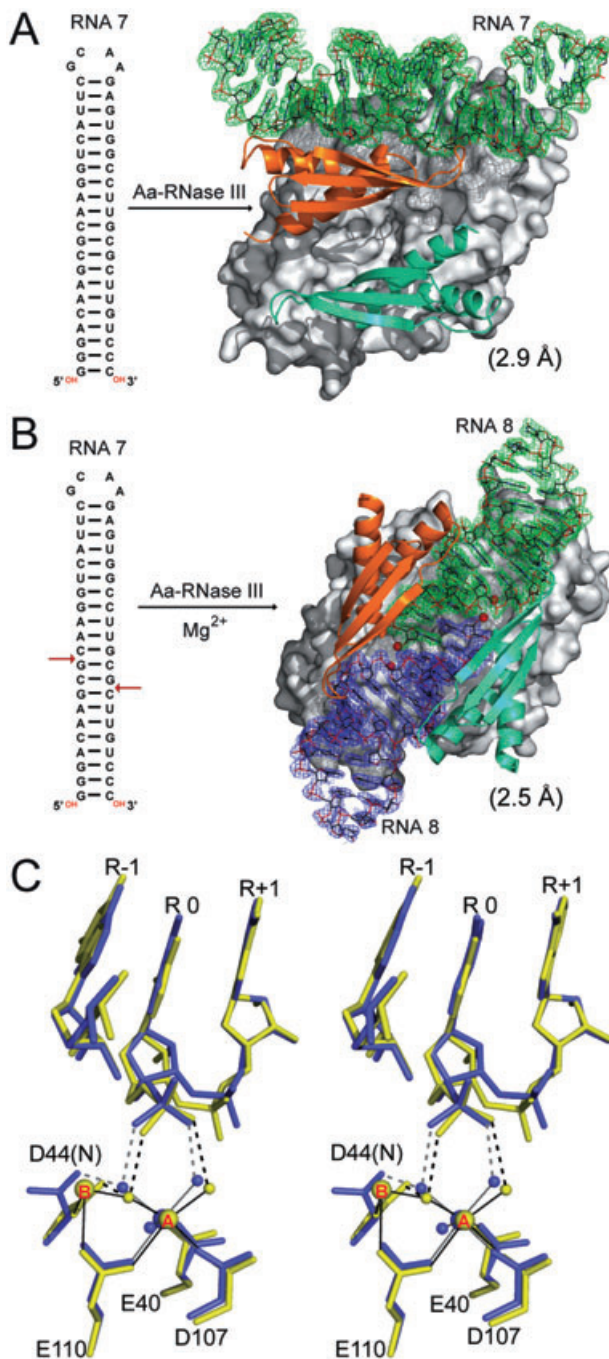
f. R_{free} is calculated from 5% of data randomly chosen not to be included in refinement.

water molecule. The distance between MgA and MgB is 4.0 Å. Comparing the structures of Aa-RNase III(D44N)–MgRNA 6 (PDB entry 2EZ6) and Aa-RNase III–MgRNA 8, the only significant difference in their catalytic sites is the side-chain conformation of residue 44 (Fig. 1C). The ~30° rotation around the CA–CB and CB–CG bonds enables the wild-type D44 side-chain in Aa-RNase III–MgRNA 8 to co-ordinate with MgB while maintaining its water-bridged

interaction with MgA. MgB has been observed in all four subunits of the two new catalytic complexes reported here. Therefore, it is the D44N mutation that hinders the binding of MgB in the Aa-RNase III(D44N)–MgRNA 6 complex (PDB entry 2EZ6).

Representative minimal product of dsRNA processing

Previously, we hypothesized that the minimal substrate for



RNase III should contain 11 base pairs (bp) in order to interact with a set of four RNA-binding motifs (RBM 1, 2, 3 and 4) in the protein (Gan *et al.*, 2006). Furthermore, a representative minimal size of the RNase III product was suggested to be a 9 bp dsRNA molecule with a 2 nt 3' overhang on each end of the duplex (Ji, 2007). RNA 8 contains 11 bp with a 4 nt loop on one end and a 2 nt 3' overhang on the other (Fig. 1B). Therefore, RNA 8 could be further processed by the enzyme, resulting in the complex of the protein with the processing products instead of RNA 8 itself.

Fig. 1. Mg²⁺ ion as a positive determinant for catalytic binding of RNA.

A. The Aa-RNase III-RNA 7 complex, containing an RNase III dimer and an RNA 7 molecule, shows that when Mg²⁺ is absent, the RNA is bound outside of the catalytic valley.

B. In the presence of Mg²⁺ ions, RNA 7 is bound inside the catalytic valley and therefore cleaved, producing RNA 8 and a small duplex; and then two RNA 8 molecules are rebound by the protein. Scissile bonds are indicated with red arrows. Four Mg²⁺ ions (two in each catalytic site) are shown as red spheres. The endoND dimer is shown as a molecular surface in grey. The two dsRBDs are shown as ribbon diagrams (helices as spirals, strand as arrows and loops as tubes) and coloured in orange and cyan respectively. RNAs are shown as stick models and outlined with the final electron density maps (2F_o - F_c, contoured at 1.0 σ level) and coloured in blue and green respectively.

C. Stereoview comparing the catalytic site in Aa-RNase III-MgRNA 8 (this work, in yellow) and that in Aa-RNase III(D44N)-MgRNA 6 (PDB entry 2EZ6, in cyan). The aa and nt residues are shown as stick models and Mg²⁺ ions and water oxygens as spheres. Metal co-ordination bonds are indicated with solid lines and hydrogen bonds with dashed lines. The nt residue in the middle is numbered 'R 0' and the rest are numbered according to the polarity of the RNA strand.

As predicted, RNA 8 was processed further when it was incubated with Aa-RNase III, producing a 9 bp dsRNA molecule with a 2 nt 3' overhang on each end of the duplex (designated as RNA 9). Interestingly, both ends of the asymmetric RNA 8 have been cleaved (Fig. 2A). In the crystal lattice, many RNA 9 molecules are stacked end-to-end, annealing their 2 nt 3' overhangs and forming pseudo-continuous duplexes (not shown). In a single Aa-RNase III-MgRNA 9 complex, two RNA 9 molecules occupy the entire length of the catalytic valley (Fig. 2B). At each end of the valley, the distal box and the first bp next to the box are recognized by RBM 4 in each subunit (Fig. 2C). RBM 4 is a loop between α-helices 5 and 6 in the endoND. The sequence of RBM 4 (₉₂FIRIKRGKINE₁₀₂) is not conserved. Neither is the interaction between the RBM and the RNA. In the Aa-RNase III(D44N)-MgRNA 6 structure, we have observed a hydrogen bond between R97 and an O2' hydroxyl of the RNA (Gan *et al.*, 2006). In the Aa-RNase III-MgRNA 9 structure, however, we have observed a hydrogen bond between K99 and an O2' hydroxyl of the RNA only at one end of the duplex (Fig. 2C). Although the interaction between N101 and the RNA is observed for both ends of the duplex, the aa residue is not conserved.

In 100 sequences of bacterial RNase III proteins, 15 residues (F15, A24, H27, L39, E40, G43, D44, G65, E110, K153, L156, Q157, Y170, F184 and A209) are strictly conserved, among which H27, D44, K153 and Q157 interact with the bound RNA. The H27 residue is located next to RBM 4; it forms a hydrogen bond with the O3' atom of nt residue R-11, which is also observed in the other two catalytically compatible complexes, Aa-RNase III(D44N)-MgRNA 6 (PDB entry 2EZ6) and Aa-RNase III-MgRNA 8. Residue D44 is located in the catalytic site; it forms a

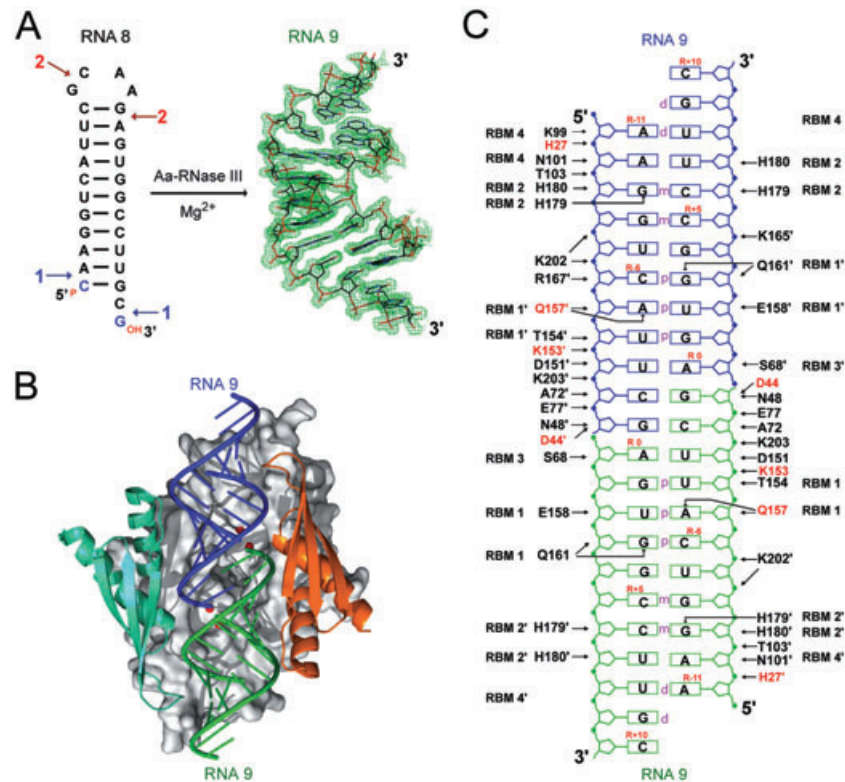


Fig. 2. A representative minimal product of dsRNA processing by bacterial RNase III.

A. A total of six nt residues, including four from the loop end (CAAG) and two from the stem end (C and G), of RNA 8 are cleaved off RNA 8 by Aa-RNase III, producing RNA 9. Scissile bonds are indicated by arrows. RNA 9 is shown as a stick model and outlined with the final electron density map ($2F_o - F_c$, contoured at 1.0σ).

B. The Aa-RNase III–MgRNA 9 complex contains an RNase III dimer and two RNA 9 molecules. The Mg^{2+} ions are shown as red spheres. The endoND dimer is shown as a molecular surface in grey. The two dsRBDs are shown as ribbon diagrams (helices as spirals, strand as arrows, and loops as tubes) and coloured in orange and cyan respectively. The two RNA 9 molecules are shown as tube-and-stick models and coloured in blue and green respectively.

C. The hydrogen bonds between the protein and the RNA observed in the Aa-RNase III–MgRNA 9 structure are schematically illustrated. For the RNA, the two RNA 9 molecules are distinguished with different colours, the protein-interacting boxes (proximal, middle and distal boxes) are indicated with one-letter abbreviations, and the two scissile bonds are located between the two RNA molecules. For the protein, the prime (') in the name of RBM (RNA-binding motif) and aa residue distinguishes between one protein subunit from the other. Residues strictly conserved in 100 RNase III sequences are highlighted in red. Hydrogen bonds between the aa and nt residues are indicated with arrows.

hydrogen bond with the O2' atom of nt residue R-1. Exactly 11 nt residues on each RNA strand are measured and defined by aa residues H27/D44' or H27'/D44, underlying the importance of the endoND dimer in the catalysis of RNase III proteins (Fig. 2C). While D44, in part, defines the scissile bond and catalyses the hydrolysis, it is H27 that dictates the length of the minimal product of bacterial RNase III. RBM 4, on the other hand, provides additional interactions between the protein and the RNA as we have previously described (Gan *et al.*, 2006). Residues K153 and Q157 are located in RBM 1 ($_{152}YKTLQEIQTQKRW_{164}$) that is the first α -helix of the dsRBD, in which residues T154, Q157, E158 and Q161 each form a hydrogen bond with an O2' hydroxyl of RNA (Gan *et al.*, 2006). As shown in Fig. 2C, K153 interacts with the phosphate bridge only, whereas Q157 also interacts with the base of R-5. However, the R-5 nt is an Ade in the Aa-RNase III–Mg RNA

9 structure but a Uri in the Aa-RNase III(D44N)–Mg RNA 6 structure (PDB entry 2EZ6), suggesting no RNA sequence specificity is imposed by Q157.

RNA-processing products and experimental conditions

RNA 7 (46-mer, Table 1) has been processed to produce RNA 8 (28-mer), and RNA 8 has been processed to produce RNA 9 (2×11 -mer), as shown in Figs 1B and 2A respectively. Prior to crystallization, the protein–RNA mixture was incubated at 75°C for 30 min. Subsequently, the reaction mixture was slowly cooled down to the room temperature when it was mixed with an equal-volume of a well (precipitant) solution to form a crystallization drop. We have been puzzled for the reasons why RNA 7 was not processed to RNA 9.

Aa-RNase III is from a thermobacterium, suggesting that the chemical reaction occurs mainly at elevated tem-

perature (75°C) during incubation (30 min). However, the only difference between the two protein–RNA solutions is the concentration of NaCl, 400 mM for RNA 7 and 100 mM for RNA 8 (Table 2), the minimal salt concentrations to keep the RNAs in solution. It remains to be tested whether the reaction is salt concentration dependent, but RNA 7 is not soluble when the concentration of NaCl drops below 400 mM.

Perhaps the reaction still continues in the crystallization drops where the concentrations of $MgCl_2$ differ between RNA 7 and RNA 8. The well solution for RNA 7 does not contain any Mg^{2+} , whereas the well solution for RNA 8 contains 200 mM $MgCl_2$ (Table 2). As the crystallization drops are made up of equal-volumes of protein solution and well solution, the Mg^{2+} concentration in the drops is 25 mM for RNA 7 but 125 mM for RNA 8. To test the Mg^{2+} concentration dependence of the reaction, we have tried to crystallize RNA 7 at the Mg^{2+} concentration for RNA 8, and vice versa, but the two experiments have not been able to produce any crystals.

Two steps towards product release

In the Aa-RNase III–MgRNA 9 structure, nt residues R 0 and R+1 exhibits alternate conformations, which has been confirmed with an additional structure determination starting with a different crystal. The two crystals diffract to similar resolutions, but the ratio between the minor and the major conformations varies slightly. At 1.7 Å resolution, the ratio for the two conformations has been estimated to be ~0.3/0.7. The entire structure has been verified vigorously with annealed omit map (Fig. 3A). The major difference between the two conformations is the position of the 5' phosphate group of R 0 (Fig. 3B). The position of the 5' phosphate in the major conformation is similar to that in the Aa-RNase III–MgRNA 8 structure, whereas that in the minor conformation is novel (Fig. 3C).

In the minor conformation, the distance between the 3' hydroxyl and the 5' phosphorus is 3.0 Å, which is shorter than the sum of the van der Waals radii of phosphorus (1.9 Å) and oxygen (1.4 Å) (Pauling, 1960), indicating that the minor conformation represents the catalytic site arrangement immediately after the phosphoryl transfer during the hydrolysis of the scissile bond (Fig. 4C). In the major conformation, the 5' phosphate has moved away from the catalytic site, suggesting that the major conformation represents a first snapshot towards product release after the reaction (Fig. 4D). A second snapshot towards product release is represented by the Aa-RNase III–MgRNA 8 structure, in which the RNA products, especially the 3' end-product, move further away from the catalytic site (Fig. 4E). In the following discussion, we refer to the three snapshots as step 0 (minor conformation of the RNA 9 complex, Fig. 4C), step 1 (major conforma-

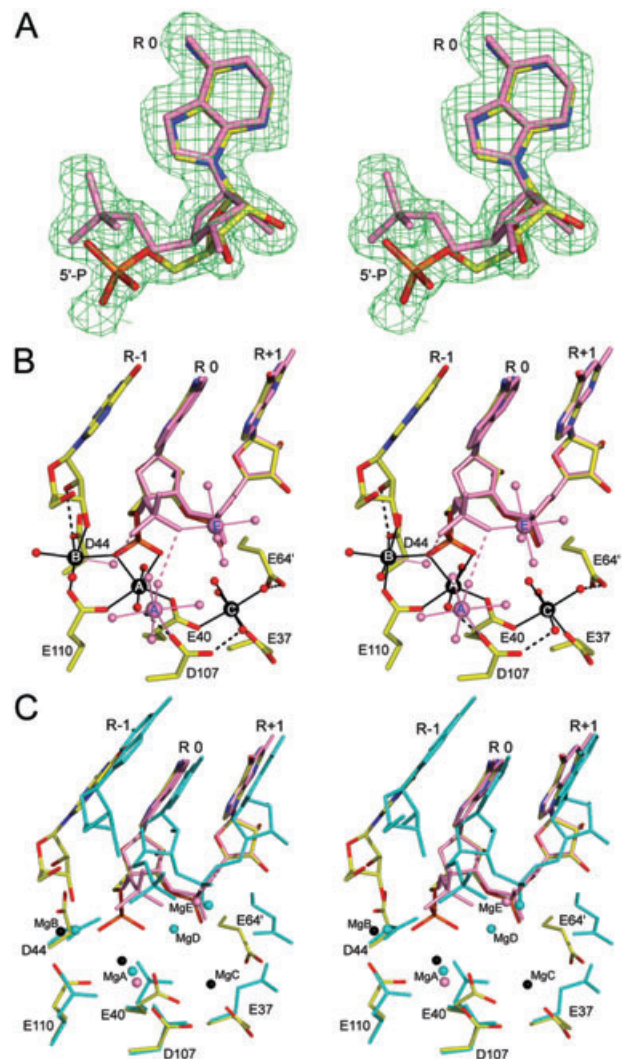


Fig. 3. Stereoviews showing the catalytic site in Aa-RNase III–MgRNA 9.

A. The alternate conformations of R 0 are outlined with the annealed omit map ($2F_o - F_c$, contoured at 1.0 σ level).

B. The catalytic site architecture is illustrated. Residues are shown as stick models and Mg^{2+} ions and water oxygens as spheres in atomic colour scheme (C, yellow; N, blue; O, red; Mg, black). The major conformation of the 5' phosphate group and associated structures are shown in pink. Solid lines indicate metal co-ordinations and dashed lines represent hydrogen bonds.

C. Superposition of the catalytic site in Aa-RNase III–MgRNA 9 (in the same colour scheme as in A) and that in Aa-RNase III–MgRNA 8 (in cyan). Water molecules, metal co-ordination bonds and hydrogen bonds are not shown for clarity. The nt residue in the middle is numbered 'R 0' and the rest are numbered according to the polarity of the RNA strand.

tion of the RNA 9 complex, Fig. 4D) and step 2 (the RNA 8 complex, Fig. 4E) towards product release.

In addition to MgA and MgB, three more Mg^{2+} ions (designated as MgC, MgD and MgE) have been observed (Fig. 3C). MgC and MgD mimic the location of MgA and MgB but shifted to the adjacent phosphodiester bond

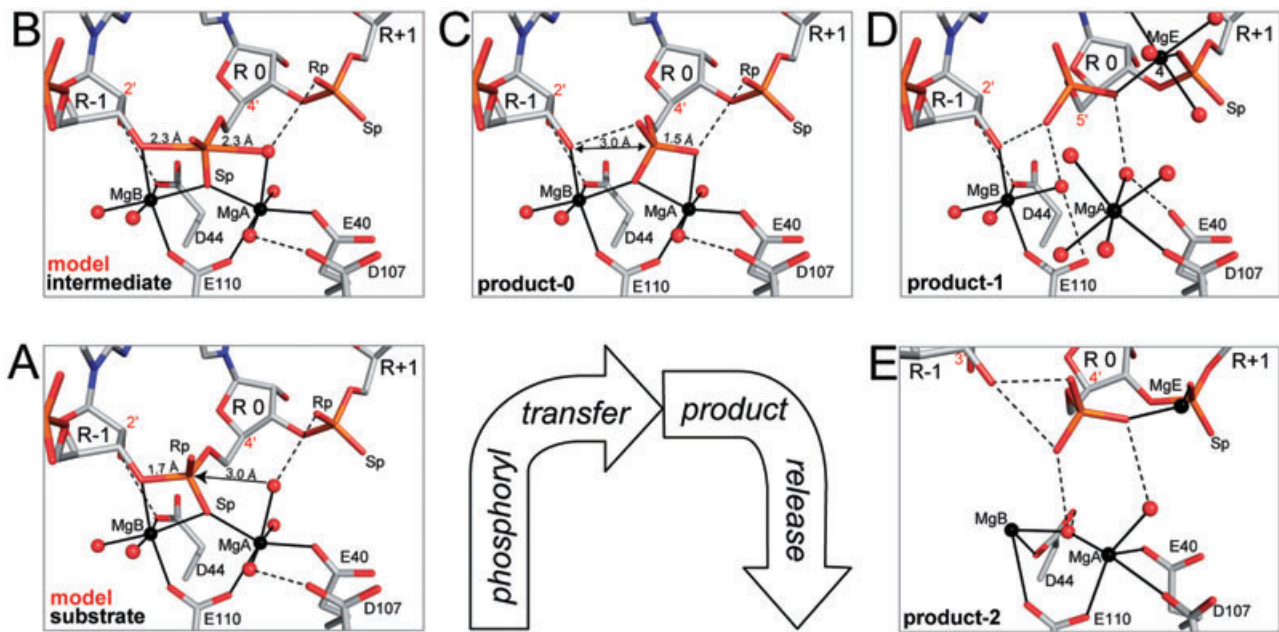


Fig. 4. Stepwise model for phosphoryl transfer and product release.

A. Model of the protein–substrate complex.

B. Model of the protein–reaction intermediate complex (transition state).

C. The catalytic site arrangement immediately after dsRNA cleavage is represented by the minor conformation of the Aa-RNase III–MgRNA 9 structure.

D. Step 1 towards product release is represented by the major conformation of the Aa-RNase III–MgRNA 9 structure.

E. Step 2 towards product release is represented by the Aa-RNase III–MgRNA 8 structure. The aa and nt residues are shown as stick models and Mg^{2+} ions and water oxygens as spheres (C, grey; N, blue; O, red; P, orange; Mg, black). Metal co-ordination bonds are illustrated as solid lines and hydrogen bonds as dashed lines. The nt residue in the middle is numbered ‘R 0’ and the rest are numbered according to the polarity of the RNA strand.

between nt residues R 0 and R+1. In the Aa-RNase III–MgRNA 9 structure, MgC co-ordinates with E37 and E40 and forms water-bridged hydrogen bonds with D107 from one subunit and E64 from the partner subunit. In the Aa-RNase III–MgRNA 8 structure, MgD co-ordinates with side-chain E40 and the phosphate oxygen Sp between nt residues R 0 and R+1. Unlike the MgA/MgB pair, MgC and MgD are not observed in both structures. Unlike the other four Mg^{2+} ions, MgE is associated with RNA only.

Three stages of phosphoryl transfer

Phosphorus is able to form five stable covalent bonds. Thus, nucleophilic attack on phosphorus could produce a relatively long-lived pentacovalent intermediate. It has been suggested that all phosphoryl transfer reactions in DNA and RNA involve the pentacovalent intermediate and inversion of the stereo configuration at the phosphorus (Burgers and Eckstein, 1979; Yang *et al.*, 2006). The minor conformation of Aa-RNase III–MgRNA 9 (Fig. 4C), a snapshot of a protein–product complex immediately after dsRNA cleavage, offers an opportunity to predict the catalytic site arrangement immediately before the reaction and the arrangement of the reaction intermediate at the transition state. On the basis of the product complex (Fig. 4C),

the intermediate (Fig. 4B, model) and the substrate (Fig. 4A, model) complexes have been derived by adjusting the torsion angles along the C4′–C5′–O5′–P–O1P chain, and breaking or making the P–O bonds. The resulting models and the product complex in the minor conformation represent three consecutive stages in the hydrolysis of a phosphodiester bond: (i) the nucleophilic attack by the MgA-activated OH^- ion on the tetrahedral ground state 5′ phosphorus (Fig. 4A, model); (ii) the formation of the trigonal bipyramidal pentavalent phosphorane intermediate (Fig. 4B, model) and (iii) the departure of the leaving group (the 3′ hydroxyl of the scissile bond) and the formation of the cleavage products (Fig. 4C).

Two- Mg^{2+} -ion catalytic mechanism

We have shown that two Mg^{2+} ions, MgA and MgB, are required for the cleavage of each phosphodiester bond. The observation of the two metal ions in each catalytic site of RNase III is a continued effort of both us and other researchers. Previously, metal site A has been suggested with Mn^{2+} (Blaszczuk *et al.*, 2001; MacRae *et al.*, 2006a), Mg^{2+} (Blaszczuk *et al.*, 2004; Gan *et al.*, 2006), Ca^{2+} (Akey and Berger, 2005) and Er^{3+} (MacRae *et al.*, 2006a), while

site B has been suggested with Mn^{2+} and Er^{3+} (MacRae *et al.*, 2006a). These observations are in agreement with existing biochemical data (Sun *et al.*, 2005). In this study, the identity of the two Mg^{2+} ions per catalytic site has been established in three steps: (i) the initial position of each Mg^{2+} was suggested as a difference Fourier peak at proper contour levels and the co-ordination geometry of the metal ion; (ii) the identity of each Mg^{2+} was verified via crystallographic refinement; in particular, the B (temperature) factor of the metal ion must be similar to that of its co-ordination atoms; and (iii) the correctness of the assignment was confirmed by the annealed omit map.

As indicated in Fig. 4A (model), MgA activates the nucleophile by lowering the pK_a of water 1 that is located 3.0 Å away from the 5' phosphorus of the scissile bond. The resulting OH^- is oriented, with the help of an electrostatic interaction with the R_P oxygen of the R+1 nt, for the in-line attack on the 5' phosphorus. MgB directly co-ordinates with the 3' leaving oxygen, facilitating the bond breakage by neutralizing the developing negative charge on this oxygen anion. Both MgA and MgB co-ordinate with the S_P oxygen of the 5' phosphate, positioning the phosphate group properly in the catalytic site and stabilizing the additional incipient negative charge in the reaction intermediate (Fig. 4B, model). MgB also co-ordinates with two water molecules that are in position to donate a proton to the 3' leaving group.

As essential residues for catalysis, E110 co-ordinates with both MgA and MgB, while D44 co-ordinates with MgB and also forms a hydrogen bond to the 2' hydroxyl group of nt R-1 (Fig. 4C). With redundant metal binding function, E40 and D107 provide needed co-ordination for MgA during catalysis. The structural arrangements of these aa residues are in agreement with their functional roles (Court, 1993; Nicholson, 1999; 2003; Sun and Nicholson, 2001; Conrad and Rauhut, 2002; Sun *et al.*, 2004; Ji, 2007).

Conformational changes of RNase III and dsRNA for catalysis

The comparative analysis between the minor conformation of the Aa-RNase III-MgRNA 9 structure (Fig. 4C) with the Aa-RNase III-MgRNA 8 structure (Fig. 4E) indicates that both the protein and the RNA exhibit significant conformational differences during catalysis (Fig. 5).

The alignment of the two structures is based on all of the C_α positions in their endoND dimers. The root-mean-square deviation (RMSD) is 0.57 Å for a total of 246 C_α positions, while it is 0.29 Å between the eight C_α positions of catalytic residues E40, D44, D107 and E110. Although the C_α positions of the eight residues align well, their side-chain conformations and the positions of the four Mg^{2+} ions differ significantly (Fig. 5A). The long axis of the dsRNA bends slightly towards the catalytic valley, but the

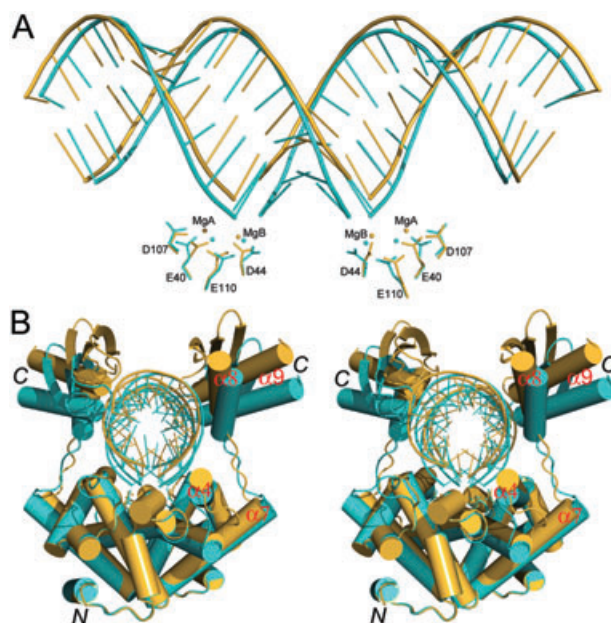


Fig. 5. Functionally relevant distortion of the dsRNA structure in the catalytic assembly.

A. The long axis of A-form dsRNA is slightly bent with the minor groove in the middle pushed towards the catalytic sites, as shown by the comparison between the minor conformation of the Aa-RNase III-MgRNA 9 structure (Fig. 4C, immediately after dsRNA cleavage, step 0 towards product release) and the Aa-RNase III-MgRNA 8 structure (Fig. 4E, step 2 towards product release).

B. Stereoview shows that the cross-section perpendicular to the long axis of A-form dsRNA is significantly distorted with the scissile bonds pulled down into the catalytic sites. The two views in A and B are related by a 90° rotation about the vertical axis. The protein-RNA complexes are shown as ribbon diagrams (helices as cylinders, strand as arrows, loops as tubes, aa side-chains as sticks, RNA as tube-and-stick models, and Mg^{2+} ions as spheres) and coloured in orange for the Aa-RNase III-MgRNA 8 structure (Fig. 4E) and in cyan for the minor conformation of the Aa-RNase III-MgRNA 9 structure (Fig. 4C). The alignment is based on all C_α positions in the endoND dimer of the two structures.

two scissile bonds appear to be 'pulled' down into the catalytic sites (Fig. 5A). How is this done?

As shown in Fig. 5B, the cross-section of the dsRNA is significantly distorted, from a circle to an ellipse. In concert with this distortion, the N-terminus of the $\alpha 4$ helix moves downwards by ~ 2.6 Å, the C-terminus of $\alpha 7$ moves outwards by ~ 2.1 Å, and the two helices in the dsRBD, $\alpha 8$ and $\alpha 9$, move downwards by ~ 5.3 and ~ 6.1 Å respectively (Fig. 5B). The RMSD for the C_α positions in a single dsRBD is ~ 0.35 Å between the two structures, suggesting that the dsRBDs move as rigid bodies; whereas the RMSD rises to ~ 3.2 Å for the C_α positions in both dsRBDs, indicating the significant change in the relative positioning of the two dsRBDs. Taken together, it indicates that the two dsRBDs can 'glide' up and down along the minor groove of the bound dsRNA. Although the upper edge of the RNA cannot be moved downwards signifi-

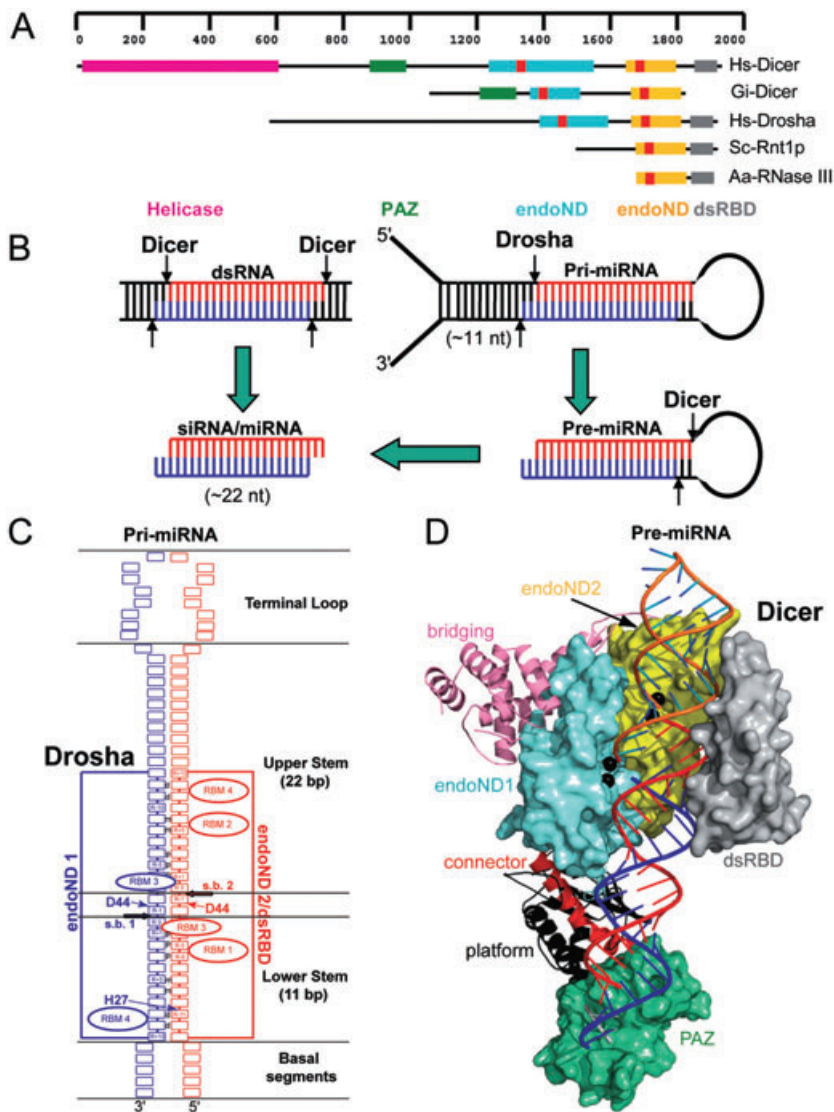


Fig. 6. How Drosha and Dicer measure. A. Domain structure of Hs-Dicer (SWISS-PROT Q9UPY3), Gi-Dicer (SWISS-PROT Q7R2M2), Hs-Drosha (SWISS-PROT Q9NRR4), Sc-Rnt1p (SWISS-PROT Q02555) and Aa-RNase III (SWISS-PROT O67082). The signature motif of RNase III proteins is indicated with a red block.

B. Typical substrate and product RNAs are illustrated for Drosha and Dicer.

C. The Drosha-RNA interactions are schematically illustrated. The pri-miRNA (primary microRNA) structure is drawn on the basis of Han *et al.* (2006). The C-terminal endoND1-endoND2-dsRBD fragment of Drosha is shown as two rectangles and labelled as 'endoND 1' and 'endoND 2/dsRBD', the RBMs (RNA-binding motifs) as ellipsoids and the pri-miRNA as a series of boxes. The two scissile bonds (s.b. 1 and s.b. 2) are indicated with block arrows, and the protein-interacting boxes in the dsRNA (proximal, middle and distal boxes) are indicated with one-letter abbreviations. The interactions between conserved residues D44 and H27 (numbering system of Aa-RNase III) and the RNA are indicated with arrows.

D. Model of the platform-to-dsRBD fragment of Dicer in complex with pre-miRNA and four Mg²⁺ ions. The platform-to-endoND2 fragment is from the Gi-Dicer-Mn²⁺ structure (PDB entry 2FFL, MacRae *et al.*, 2006b). The Mg²⁺ ions, dsRBD and RNA is from the Aa-RNase III-MgRNA 8 structure with an extension of the RNA to include a typical siRNA/miRNA that contains a 20 bp A-form dsRNA with a 2 nt 3' overhang on each end of the duplex. The PAZ domain, the two endoNDs, and the dsRBD are shown as molecular surfaces (in green, cyan, yellow and grey respectively); the platform domain, the connector, and the bridging domain are shown as ribbon diagrams (in black, red and pink respectively). The 2 nt RNA segment in grey on the PAZ domain indicates the anchoring site for the 2 nt 3' overhang of the pre-miRNA as suggested by the structure of a PAZ domain in complex with a dsRNA (Ma *et al.*, 2004). The Mg²⁺ ions are shown as black spheres.

cantly, the flexibility of the RNA allows the two scissile bonds to be 'squeezed' into the catalytic sites where hydrolysis is supposed to occur (Fig. 5B).

Implications for the mechanism of eukaryotic RNase III

The RNase III family can be represented by four members, including bacterial RNase III and eukaryotic Rnt1p, Drosha and Dicer, among which the endoND is strictly conserved (Fig. 6A). All reported structures show that two endoNDs form a tight dimer (Ji, 2007). Aa-RNase III contains one endoND; the endoNDs from two molecules form a tight dimer. Gi-Dicer has two endoNDs; the two endoNDs dimerize intramolecularly (MacRae *et al.*, 2006a). The endoND dimer of known RNase III structures superimpose well, leading to virtually identical positioning

of catalytically important residues, including D44 and E110, which is the structural basis for the hallmarks of RNase III products, including the 3'-hydroxyl and 5'-phosphate ends and the 2 nt 3' overhang. Therefore, the eukaryotic Rnt1p, Drosha and Dicer must follow the same mechanism of dsRNA hydrolysis as described for the bacterial RNase III, although every family member exhibits distinct substrate specificity and product length.

While most RNase III proteins recognize long dsRNA in a similar fashion, each family member possesses additional mechanism of substrate specificity towards hairpin RNAs. Bacterial RNase III selects its hairpin substrates, at least in part, through anti-determinant nt (Zhang and Nicholson, 1997; Pertzev and Nicholson, 2006). The hairpin substrates of Rnt1p contain an NGNN tetraloop, in which the G is universally conserved; deletion

of the loop or changing the G to any other nt blocks all cleavage and most binding activities of the enzyme (Lamontagne *et al.*, 2003). For Droscha, however, the terminal loop of primary microRNA (pri-miRNA, Fig. 6B) is nonessential, but the first bp following its flanking single-stranded RNA (ssRNA) segments is critical for both recognition and processing (Han *et al.*, 2006). Finally, Dicer recognizes the 2 nt 3' overhang in the product of Droscha (pre-miRNA, Fig. 6B) but cannot process pri-miRNA directly (Lee *et al.*, 2003). The aa residues required for their selectivity have not been fully elucidated.

Droscha processes pri-miRNAs that typically consist of a ~33 bp stem with a terminal loop on one end and flanking single-stranded segments on the other (Lee *et al.*, 2003). The scissile bond is determined mainly by the distance of 11 nt from the stem-ssRNA junction (Han *et al.*, 2006). Interestingly, residue H27, which defines the minimal product length for bacterial RNase III, is also conserved in the first endoND (endoND 1) of Droscha from human, fruit fly, mouse, chicken, zebrafish and green puffer (Swiss-Prot entries Q9NRR4, Q7KNF1, Q5HZJ0, Q5ZIR3, A2RV16 and Q4SKW1 respectively). As illustrated in Fig. 6C, this residue may recognize the R-11 nt near the 5' end and thus define the distance of 11 nt from the stem-ssRNA junction. For Dicer, however, a different measuring mechanism must be employed because the siRNAs (RNA duplexes of ~20 bp with a 2 nt 3' overhang on each end) are double the length of RNA 9 and thus beyond the reach of RBM 4 and H27. Although no structure of any Dicer-RNA complex is available to prove the point, a model complex can be constructed on the basis of available structures, suggesting that the length of a typical siRNA (an RNA duplex of 20 bp with a 2 nt 3' overhang on each end) approximately equals the distance between the catalytic sites and the 2 nt 3' overhang-anchoring site on the PAZ domain (Fig. 6D). Although residue H27 is conserved in the second endoND (endoND 2) of 10 Dicer sequences we have examined, the functional role of this residue remains to be elucidated. Residue H27 is not conserved in Rnt1p, and the cleavage site in the substrate of Rnt1p is about 14–16 nt from the tetraloop (Lamontagne *et al.*, 2001). The measuring mechanism of Rnt1p is not clear.

Most RNase III proteins are multifunctional. Bacterial RNase III can function as either a dsRNA-processing enzyme, which cleaves dsRNA into small duplexes, or a dsRNA-binding protein, which binds, stabilizes and thus suppresses the expression of certain RNAs without cleaving them. In addition to processing dsRNA into siRNA, Dicer helps in loading the siRNA into the RNA-induced silencing complex (RISC) (MacRae *et al.*, 2006b). Recently, it has been shown that Rnt1p can bind short RNA transcripts and use them as guides for sequence-specific RNA cleavage (Lamontagne and Abou Elela, 2007). For Droscha, which converts the pri-miRNA into pre-miRNA, no

additional function has been reported to date. It appears that both bacterial RNase III and Rnt1p are capable of carrying out gene silencing activity without the requirement of downstream RISC or RISC-like multi-protein complexes.

Conclusions

The structural data presented in this study show that for the assembling of a catalytically competent protein-RNA complex, Mg^{2+} is essential and conformational changes in both the substrate and the protein are critical. Also revealed is the catalytic site arrangement of an RNase III-dsRNA complex immediately after the phosphoryl transfer reaction (Fig. 4C) followed by two more snapshots of the protein-product complex as it progresses towards product release (Fig. 4D and E). On the basis of the catalytic site structure immediately after the phosphoryl transfer, a protein-substrate model (Fig. 4A) and a protein-reaction intermediate model (Fig. 4B) have been constructed. Together, the structures and models predict a stepwise picture of the two- Mg^{2+} -ion catalytic mechanism for the hydrolysis of each phosphodiester bond, which generates the 3'-hydroxyl and 5'-phosphate ends. The cleavage of both strands of a dsRNA substrate creates the 2 nt 3' overhang in the product. This mechanism is universally applicable to all members of the RNase III family.

Residue H27 is strictly conserved in 100 bacterial RNase III sequences. On each RNA strand, H27 from one subunit forms a hydrogen bond with the O3' atom of nt residue R-11, and residue D44 from the partner subunit forms a hydrogen bond with the O2' atom of nt residue R-1. Thus, an exact 11 nt length is defined by these two residues of the endoND dimer. While D44 participates in the hydrolysis of the phosphodiester bond, it is H27 that dictates the length of the minimal product of bacterial RNase III such as RNA 9 (Fig. 2C). H27 is not conserved in Rnt1p, but it is conserved in the endoND 1 of 6 Droscha sequences and the endoND 2 of 10 Dicer sequences which we have examined. In Droscha, this residue appears to recognize the R-11 nt near the 5' end and thus define the distance of 11 nt from the stem-ssRNA junction (Fig. 6C) although its role in Dicer is not clear.

Experimental procedures

Aa-RNase III was prepared as described (Gan *et al.*, 2005). RNA 7 (Fig. 1) was derived in part from the R1.1[WC] var-7 RNA (Zhang and Nicholson, 1997). Prior to crystallization, the protein-RNA mixture was incubated in the presence of Mg^{2+} (Table 2) at 75°C for 30 min. Subsequently, the reaction mixture was slowly cooled down to the room temperature.

Crystallization conditions (Table 2) were identified with a Hydra II Plus One robot system (Matrix Technologies Corporation) using the sitting-drop vapour diffusion method at $19 \pm 1^\circ\text{C}$. X-ray diffraction data were collected at cryogenic

temperature at the South-east Regional Collaborative Access Team (SER-CAT) insertion device beamline 22 (22-ID) equipped with a Mar-300 CCD detector at the Advanced Photon Source (APS), Argonne National Laboratory. Data processing was carried out with HKL2000 (Otwinowski and Minor, 1997). Data statistics were summarized in Table 2.

The three structures were solved with molecular replacement using either AMoRe (Navaza, 1994) or PHASER (Reed, 2000). The initial models were subjected to rigid body refinement, energy minimization and grouped B-factor refinement followed by a difference Fourier synthesis, which revealed the position of RNA. The structures were refined with CNS (Brünger *et al.*, 1998). Approximately 5% reflections were randomly selected for cross validation (R_{free}). Bulk solvent correction was employed. The structures were verified with the annealed omit map (Brünger *et al.*, 1998) and assessed with PROCHECK (Laskowski *et al.*, 1993) and WHAT IF (Vriend, 1990). The refinement statistics were summarized in Table 2. All graphics work was carried out using O (Jones *et al.*, 1991). Illustrations were prepared with PyMOL (DeLano, 2002).

The protein–substrate (Fig. 4A, model) and the protein–reaction intermediate (Fig. 4B, model) complexes were derived on the basis of the protein–product structure immediately after the phosphoryl transfer (Fig. 4C) by adjusting the torsion angles along the C4′–C5′–O5′–P–O1P chain, and breaking or making the corresponding P–O bonds. No energy minimization was necessary because the structural alterations were minimal. The co-ordinates are available from the corresponding author upon request.

The co-ordinates and structure factors for the three crystal structures have been deposited in the RCSB Protein Data Bank under the accession codes 2NUE (Aa-RNase III RNA 7), 2NUF (Aa-RNase III–MgRNA 8) and 2NUG (Aa-RNase III–MgRNA 9).

Acknowledgements

We thank Allen Nicholson and Alexander Wlodawer for discussion and reading the manuscript. X-ray diffraction data were collected at the SER-CAT 22-ID beamline of the APS, Argonne National Laboratory. Supporting institutions may be found at <http://www.ser-cat.org/members.html>. This research was supported by the Intramural Research Program of the NIH, National Cancer Institute, Center for Cancer Research.

References

- Akey, D.L., and Berger, J.M. (2005) Structure of the nuclease domain of ribonuclease III from *M. tuberculosis* at 2.1 Å. *Protein Sci* **14**: 2744–2750.
- Bernstein, E., Caudy, A.A., Hammond, S.M., and Hannon, G.J. (2001) Role for a bidentate ribonuclease in the initiation step of RNA interference. *Nature* **409**: 363–366.
- Blaszczyk, J., Tropea, J.E., Bubunenko, M., Rutzahn, K.M., Waugh, D.S., Court, D.L., and Ji, X. (2001) Crystallographic and modeling studies of RNase III suggest a mechanism for double-stranded RNA cleavage. *Structure* **9**: 1225–1236.
- Blaszczyk, J., Gan, J., Tropea, J.E., Court, D.L., Waugh, D.S., and Ji, X. (2004) Noncatalytic assembly of ribonu-

- lease III with double-stranded RNA. *Structure (Camb)* **12**: 457–466.
- Brünger, A.T., Adams, P.D., Clore, G.M., DeLano, W.L., Gros, P., Grosse-Kunstleve, R.W., *et al.* (1998) Crystallography & NMR system: a new software suite for macromolecular structure determination. *Acta Crystallogr D* **54**: 905–921.
- Burgers, P.M., and Eckstein, F. (1979) Stereochemistry of internucleotide bond formation by polynucleotide phosphorylase from *Micrococcus luteus*. *Biochemistry* **18**: 450–454.
- Calin-Jageman, I., and Nicholson, A.W. (2003) RNA structure-dependent uncoupling of substrate recognition and cleavage by *Escherichia coli* ribonuclease III. *Nucleic Acids Res* **31**: 2381–2392.
- Calin-Jageman, I., Amarasinghe, A.K., and Nicholson, A.W. (2001) Ethidium-dependent uncoupling of substrate binding and cleavage by *Escherichia coli* ribonuclease III. *Nucleic Acids Res* **29**: 1915–1925.
- Carthew, R.W. (2001) Gene silencing by double-stranded RNA. *Curr Opin Cell Biol* **13**: 244–248.
- Conrad, C., and Rauhut, R. (2002) Ribonuclease III: new sense from nuisance. *Int J Biochem Cell Biol* **34**: 116–129.
- Court, D.L. (1993) RNA processing and degradation by RNase III. In *Control of Messenger RNA Stability*. Belasco, J.G., and Brawerman, G. (eds). New York: Academic Press, pp. 71–116.
- Dasgupta, S., Fernandez, L., Kameyama, L., Inada, T., Nakamura, Y., Pappas, A., and Court, D.L. (1998) Genetic uncoupling of the dsRNA-binding and RNA cleavage activities of the *Escherichia coli* endoribonuclease RNase III – the effect of dsRNA binding on gene expression. *Mol Microbiol* **28**: 629–640.
- Davies, D.R., Goryshin, I.Y., Reznikoff, W.S., and Rayment, I. (2000) Three-dimensional structure of the Tn5 synaptic complex transposition intermediate. *Science* **289**: 77–85.
- DeLano, W.L. (2002) *The PyMOL Molecular Graphics System*. San Carlos, CA: Delano Scientific.
- Filippov, V., Solov'yev, V., Filippova, M., and Gill, S.S. (2000) A novel type of RNase III family proteins in eukaryotes. *Gene* **245**: 213–221.
- Gan, J., Tropea, J.E., Austin, B.P., Court, D.L., Waugh, D.S., and Ji, X. (2005) Intermediate states of ribonuclease III in complex with double-stranded RNA. *Structure (Camb)* **13**: 1435–1442.
- Gan, J., Tropea, J.E., Austin, B.P., Court, D.L., Waugh, D.S., and Ji, X. (2006) Structural insight into the mechanism of double-stranded RNA processing by ribonuclease III. *Cell* **124**: 355–366.
- Guarneros, G. (1988) Retroregulation of bacteriophage lambda int gene expression. *Curr Top Microbiol Immunol* **136**: 1–19.
- Han, J., Lee, Y., Yeom, K.H., Nam, J.W., Heo, I., Rhee, J.K., *et al.* (2006) Molecular basis for the recognition of primary microRNAs by the Drosha-DGCR8 complex. *Cell* **125**: 887–901.
- Inada, T., and Nakamura, Y. (1995) Lethal double-stranded RNA processing activity of ribonuclease III in the absence of suhB protein of *Escherichia coli*. *Biochimie* **77**: 294–302.
- Ji, X. (2006) Structural basis for non-catalytic and catalytic activities of ribonuclease III. *Acta Crystallogr D* **62**: 933–940.

- Ji, X. (2007) The mechanism of RNase III action: how dicer dices. In *RNAi Edition of Current Topics in Microbiology and Immunology*. Paddison, P.J., and Vogt, P.K. (eds). New York: Springer Publishers, pp. 99–116.
- Jones, T.A., Zou, J.Y., Cowan, S.W., and Kjeldgaard, M. (1991) Improved methods for building protein models in electron density maps and the location of errors in these models. *Acta Crystallogr A* **47**: 110–119.
- Krainer, A. (1997) *Eukaryotic mRNA Processing*. New York: IRL Press.
- Lamontagne, B., and Abou Elela, S. (2007) Short RNA guides cleavage by eukaryotic RNase III. *PLoS ONE* **2**: e472.
- Lamontagne, B., Larose, S., Boulanger, J., and Elela, S.A. (2001) The RNase III family: a conserved structure and expanding functions in eukaryotic dsRNA metabolism. *Curr Issues Mol Biol* **3**: 71–78.
- Lamontagne, B., Ghazal, G., Lebars, I., Yoshizawa, S., Fourmy, D., and Elela, S.A. (2003) Sequence dependence of substrate recognition and cleavage by yeast RNase III. *J Mol Biol* **327**: 985–1000.
- Laskowski, R.A., MacArthur, M.W., Moss, D.S., and Thornton, J.M. (1993) PROCHECK: a program to check stereochemical quality of protein structures. *J Appl Crystallogr* **26**: 283–291.
- Lee, Y., Ahn, C., Han, J., Choi, H., Kim, J., Yim, J., et al. (2003) The nuclear RNase III Drosha initiates microRNA processing. *Nature* **425**: 415–419.
- Ma, J.B., Ye, K., and Patel, D.J. (2004) Structural basis for overhang-specific small interfering RNA recognition by the PAZ domain. *Nature* **429**: 318–322.
- MacRae, I.J., Zhou, K., Li, F., Repic, A., Brooks, A.N., Cande, W.Z., et al. (2006a) Structural basis for double-stranded RNA processing by dicer. *Science* **311**: 195–198.
- MacRae, I.J., Li, F., Zhou, K., Cande, W.Z., and Doudna, J.A. (2006b) Structure of dicer and mechanistic implications for RNAi. *Cold Spring Harb Symp Quant Biol* **71**: 73–80.
- Navaza, J. (1994) An automated package for molecular replacement. *Acta Crystallogr A* **50**: 157–163.
- Nicholson, A.W. (1996) Structure, reactivity, and biology of double-stranded RNA. *Prog Nucleic Acid Res Mol Biol* **52**: 1–65.
- Nicholson, A.W. (1999) Function, mechanism and regulation of bacterial ribonucleases. *FEMS Microbiol Rev* **23**: 371–390.
- Nicholson, A.W. (2003) The ribonuclease superfamily: forms and functions in RNA maturation, decay, and gene silencing. In *RNAi: A Guide to Gene Silencing*. Hannon, G.J. (ed.). Cold Spring Harbor, NY: Cold Spring Harbor Laboratory Press, pp. 149–174.
- Nowotny, M., and Yang, W. (2006) Stepwise analyses of metal ions in RNase H catalysis from substrate destabilization to product release. *EMBO J* **25**: 1924–1933.
- Nowotny, M., Gaidamakov, S.A., Crouch, R.J., and Yang, W. (2005) Crystal structures of RNase H bound to an RNA/DNA hybrid: substrate specificity and metal-dependent catalysis. *Cell* **121**: 1005–1016.
- Oppenheim, A.B., Kornitzer, D., Altuvia, S., and Court, D.L. (1993) Posttranscriptional control of the lysogenic pathway in bacteriophage lambda. *Prog Nucleic Acid Res Mol Biol* **46**: 37–49.
- Otwinowski, Z., and Minor, W. (1997) Processing of X-ray diffraction data collected in oscillation mode. *Methods Enzymol* **276**: 307–326.
- Pauling, L. (1960) *The Nature of the Chemical Bond*. Ithaca, NY: Cornell University Press.
- Pertzev, A.V., and Nicholson, A.W. (2006) Characterization of RNA sequence determinants and antideterminants of processing reactivity for a minimal substrate of *Escherichia coli* ribonuclease III. *Nucleic Acids Res* **34**: 3708–3721.
- Reed, R.J. (2000) Pushing the boundaries of molecular replacement with maximum likelihood. *Acta Crystallogr D* **57**: 1373–1382.
- van Rij, R.P., and Andino, R. (2006) The silent treatment: RNAi as a defense against virus infection in mammals. *Trends Biotechnol* **24**: 186–193.
- Robertson, H.D., Webster, R.E., and Zinder, N.D. (1968) Purification and properties of ribonuclease III from *Escherichia coli*. *J Biol Chem* **243**: 82–91.
- Saleh, M.C., Van Rij, R.P., and Andino, R. (2004) RNA silencing in viral infections: insights from poliovirus. *Virus Res* **102**: 11–17.
- Steiniger-White, M., Rayment, I., and Reznikoff, W.S. (2004) Structure/function insights into Tn5 transposition. *Curr Opin Struct Biol* **14**: 50–57.
- Sun, W., and Nicholson, A.W. (2001) Mechanism of action of *Escherichia coli* ribonuclease III. Stringent chemical requirement for the glutamic acid 117 side chain and Mn(2+) rescue of the Glu117Asp mutant. *Biochemistry* **40**: 5102–5110.
- Sun, W., Li, G., and Nicholson, A.W. (2004) Mutational analysis of the nuclease domain of *Escherichia coli* ribonuclease III. Identification of conserved acidic residues that are important for catalytic function in vitro. *Biochemistry* **43**: 13054–13062.
- Sun, W., Pertzev, A., and Nicholson, A.W. (2005) Catalytic mechanism of *Escherichia coli* ribonuclease III: kinetic and inhibitor evidence for the involvement of two magnesium ions in RNA phosphodiester hydrolysis. *Nucleic Acids Res* **33**: 807–815.
- Vriend, G. (1990) WHAT IF: a molecular modeling and drug design program. *J Mol Graph* **8**: 52–56, 29.
- Wu, H., Xu, H., Miraglia, L.J., and Croke, S.T. (2000) Human RNase III is a 160-kDa protein involved in preribosomal RNA processing. *J Biol Chem* **275**: 36957–36965.
- Yang, D., Buchholz, F., Huang, Z., Goga, A., Chen, C.Y., Brodsky, F.M., and Bishop, J.M. (2002) Short RNA duplexes produced by hydrolysis with *Escherichia coli* RNase III mediate effective RNA interference in mammalian cells. *Proc Natl Acad Sci USA* **99**: 9942–9947.
- Yang, W., Lee, J.Y., and Nowotny, M. (2006) Making and breaking nucleic acids: two-Mg²⁺-ion catalysis and substrate specificity. *Mol Cell* **22**: 5–13.
- Zhang, K., and Nicholson, A.W. (1997) Regulation of ribonuclease III processing by double-helical sequence antideterminants. *Proc Natl Acad Sci USA* **94**: 13437–13441.